

Retrieving positions of closely packed sub-wavelength nanoparticles from their diffraction patterns

Benquan Wang^{1,2}, Ruyi An³, Eng Aik Chan^{1,2*}, Giorgio Adamo^{1,2}, Jin-Kyu So^{1,2}, Yewen Li³
Zexiang Shen^{1,2}, Bo An³ and Nikolay I. Zheludev^{1,2,4}

¹ Centre for Disruptive Photonic Technologies, TPI, Nanyang Technological University, 21 Nanyang Link, Singapore 637371, Singapore

² Division of Physics and Applied Physics, School of Physical and Mathematical Science, Nanyang Technological University, Singapore 637371, Singapore

³ School of Computer Science and Engineering, Nanyang Technological University, Singapore 639798, Singapore

⁴ Centre for Photonics Metamaterials and Optoelectronics Research Centre, University of Southampton, Southampton SO17 1BJ, UK

*Author to whom correspondence should be addressed: echan003@e.ntu.edu.sg

Distinguishing two objects or point sources located closer than the Rayleigh distance is impossible in conventional microscopy. Understandably, the task becomes increasingly harder with a growing number of particles placed in close proximity. It has been recently demonstrated that subwavelength nanoparticles in closely packed clusters can be counted by AI-enabled analysis of the diffraction patterns of coherent light scattered by the cluster. Here, we show that deep learning analysis can return the actual positions of nanoparticles in the cluster. The Pearson correlation coefficient between the ground truth and reconstructed positions of nanoparticles exceeds 0.7 for clusters of 10 nanoparticles and 0.8 for clusters of two nanoparticles of 0.16λ in diameter, even if they are separated by distances below the Rayleigh resolution limit of 0.68λ corresponding to a lens with numerical aperture $NA=0.9$.

Imaging, localization, and retrieval of the number of subwavelength objects closely packed, although extremely challenging, is a problem that is very often encountered in applications such as environmental monitoring¹, semiconductor optical inspection², materials³, and biomedical analysis⁴. This problem can't be tackled by conventional microscopy, which is bound by the Abbe-Rayleigh diffraction limit to a resolution of about half the wavelength of the incident light. Improved resolution can be obtained by using optical techniques such as PALM and STED, which work with photoactivated labels⁵⁻⁷ or near-field methods^{8,9}, which require contact with the sample and are therefore unsuitable in many instances because of their complexity and invasiveness¹⁰.

It was recently reported that deep learning-enabled analysis of single-shot diffraction patterns of coherent light scattered by subwavelength objects can be used to obtain unlabeled super-resolution optical metrology^{11,12} and to correctly predict the number of nano-objects in clusters of subwavelength objects¹³. Here, we show that AI-empowered analysis of the optical diffraction patterns of closely packed subwavelength nanoholes, using a neural network trained on similar *a priori* known objects, allows us to retrieve their positions, even when the nanoholes are touching.

We conducted numerical experiments using a coherent plane-wave illumination ($\lambda = 633$ nm) of clusters of subwavelength nanoholes with a diameter of $\lambda/6.33$ perforated in an opaque film, randomly placed within a $2.2\lambda \times 2.2\lambda$ area. We image the diffraction patterns created by the nanoholes clusters at a distance, $H = 1\lambda$

away from the sample, over a $22\lambda \times 22\lambda$ field of view, accounting for the numerical aperture, $NA = 0.9$ of a real imaging system (Fig. 1a). Pairs of the far-field diffraction pattern and the corresponding position map of nanoholes in the cluster were used to train a modified U-Net encoder-decoder convolutional neural network. U-Net is a convolutional neural network (CNN) architecture specifically designed for semantic image segmentation¹⁴, i.e., categorizing each pixel in an image into a class or object, which continues to generate widespread interest and has found application in medical imaging¹⁵ and optical microscopy¹⁶. The network has a U-shaped architecture consisting of an encoder, or dimension-reducing path, followed by a decoder or dimension-increasing path, with a symmetric design that reduces the risk of information loss during the encoding and decoding processes¹⁷. The encoder path captures and condenses information of inputs at multiple levels of abstraction through convolutional and pooling layers, as in traditional CNNs¹⁸. The decoder path, instead, uses transposed convolutions to recover the dimension, conditioned by skip connections from the correspondingly encoded information at the same level. This approach enables the network to produce precise segmentation masks and effectively addresses the vanishing gradient problem¹⁹. This phenomenon, where the network loses its capacity to capture long-term dependencies, is mitigated through this design. To promote efficient information propagation and resolve the category imbalance challenge in the particle localization problem (i.e., the small fraction of nanoholes with respect to the background), we modify the U-Net by introducing a residual architecture²⁰ with multiple deep

This is the author's peer reviewed, accepted manuscript. However, the online version of record will be different from this version once it has been copyedited and typeset.

PLEASE CITE THIS ARTICLE AS DOI: 10.1063/5.0194393

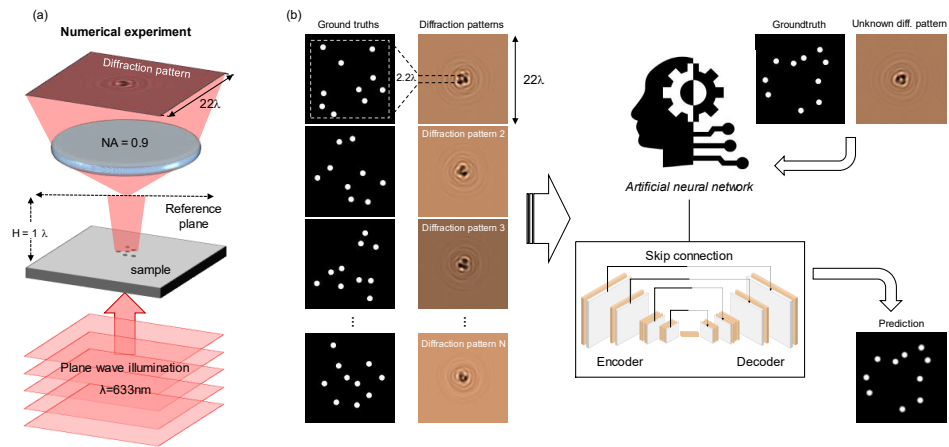


Figure 1. (a) Schematic of the numerical experiment. Clusters of subwavelength nanoholes with diameters of $\lambda/6.33$, placed within a $2.2 \lambda \times 2.2 \lambda$ area in a 100 nm-thick chromium film, are illuminated by a plane wave with wavelength = 633 nm. The diffraction pattern of the scattered light intensity, at a distance, $H = 1\lambda$, is recorded with a numerical aperture, $NA = 0.9$. (b) Pairs of diffraction patterns and corresponding position maps of the nanoholes (ground truths) are used to train a modified U-Net, encoder-decoder convolutional neural network, which will then be able to retrieve the positions of nanoholes from single-shot unknown diffraction patterns.

convolutional layers and novel hybrid loss function that combines Binary Cross-Entropy loss and a Class-Balanced loss (details in Supplementary Material Sections 1- 5). The trained network is then able to retrieve the positions of the particle in the cluster from previously unseen diffraction patterns (Fig.1b).

Each sample contains up to 10 nanoholes that may form clusters with an inter-particle distance smaller than the Rayleigh limit of resolution of a conventional microscope, $0.61 \lambda/NA$. We define the sizes of the sub-Rayleigh clusters by counting the number of nanoholes whose inter-particle distance is smaller than the Rayleigh

limit (Fig. 2a) and characterize each sample by the largest sub-Rayleigh cluster size within the $2.2 \lambda \times 2.2 \lambda$ area. It shall be noted how, often, not only pairs but all particles fall within the Rayleigh distance (e.g., nanoholes A, B, C in Fig 2a). The groundtruth maps used to supervise the network are binary images of 512×512 pixels size (corresponding to an area of $2.5 \lambda \times 2.5 \lambda$) where white pixels (value = 1) represent the nanoholes and black pixels (value = 0) represent the Cr film (second column in Fig. 2b). The corresponding diffraction patterns were generated plotting the total electric field intensity profiles calculated by finite-difference-time-domain (FDTD) full

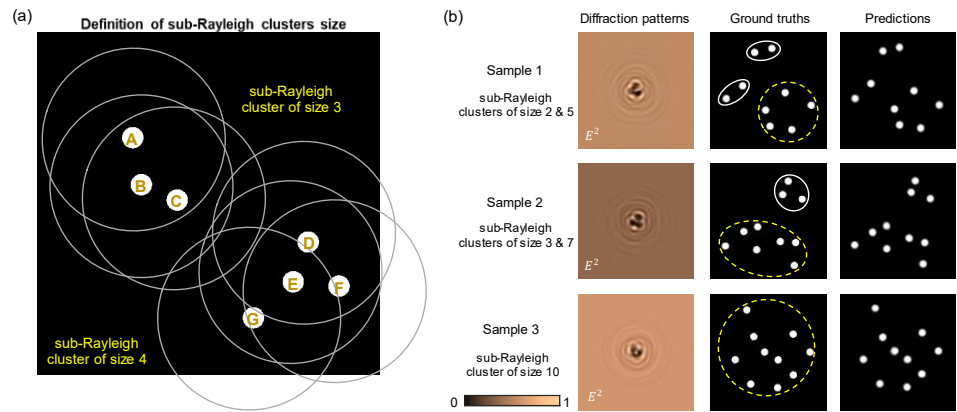


Figure 2. (a) A group of nanoholes is identified as a sub-Rayleigh cluster if each nanohole in the cluster has at least one neighboring nanohole within Rayleigh distance, $0.61 \lambda/NA$. The binary map shown here contains a sub-Rayleigh cluster of 3 nanoholes (A, B, C) and a cluster of 4 nanoholes (D, E, F, G). The circles represent the Rayleigh region of each nanohole. Nanoholes (A, B, C) and nanoholes (D, E, F) all fall within the Rayleigh distance. (b) Diffraction patterns (first column), groundtruth (second column) and prediction (third column) images of three samples where the size of the largest Rayleigh cluster (yellow dashed circle) increases from 5 (first row), to 7 (second row) and 10 (third row).

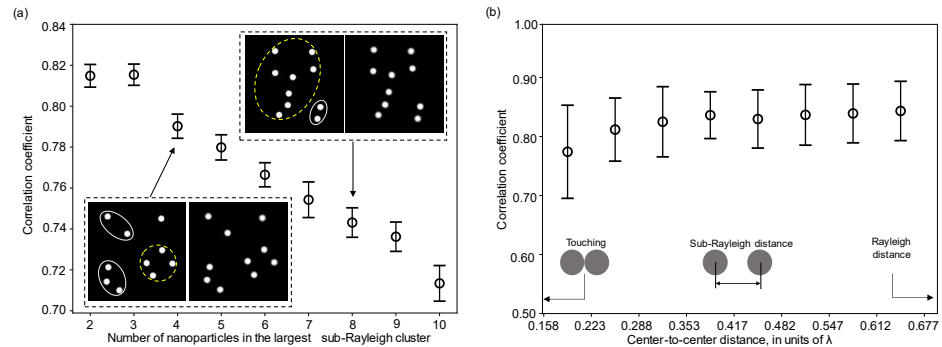


Figure 3. (a) Pearson correlation coefficient between the predicted and ground truth images as a function of the sub-Rayleigh cluster size. Insets: examples of ground truth (left) and prediction (right) images for samples with the largest sub-Rayleigh cluster size of 4 (lower left) and 8 (upper right) nanoholes. (b) Pearson correlation coefficient between the predicted and ground truth images for the typical Rayleigh diffraction case, two closely spaced nanoholes of decreasing center-to-center distance.

Maxwell solver (Supplementary Material Section 6), at a distance of 1λ from the sample surface, over a field of view of $22 \lambda \times 22 \lambda$ (first column in Fig. 2b). Fig. 2b shows that the light propagating through the nanoholes, generated very rich interference patterns in the diffraction maps, thus making it very difficult to correlate to a specific number and distribution of nanoholes on the sample. Nonetheless, the trained network can not only retrieve the number and positions of the nanoholes in the clusters but also return 512×512 pixels images (third column in Fig. 2b) where the sizes of the nanoholes match well those of the ground truth and therefore can be regarded as a form of super-resolution imaging.

A total of 11,700 samples and corresponding diffraction patterns were generated for the numerical experiment, of which 7,200 were used for training, 1800 for validation, and 2,700 for testing (Supplementary Material Section 7). We use the Pearson correlation coefficient²¹ between the predicted and ground truth images to evaluate the accuracy of image reconstruction of our technique.

$$r_{xy} = \frac{\sum_{i=1}^n (x_i - \bar{x})(y_i - \bar{y})}{\sqrt{\sum_{i=1}^n (x_i - \bar{x})^2} \sqrt{\sum_{i=1}^n (y_i - \bar{y})^2}} \quad (1)$$

where n is the sample size, x_i , y_i are the individual sample points in our reconstructed image and ground truth image, respectively, indexed with i , $\bar{x} = \frac{1}{n} \sum_{i=1}^n x_i$ (the sample mean), and analogously for \bar{y} .

Fig. 3a shows that the accuracy exceeds 0.81 for samples with the sub-Rayleigh cluster index of 3 and remains as high as 0.71 for samples containing 10 nanoholes within the same sub-Rayleigh cluster, which is an indication of the trained network's robustness against the size of sub-Rayleigh clusters. The decrement of the image reconstruction accuracy with the increasing size of sub-Rayleigh clusters can be justified by the increase in the complexity of the interference patterns.

To explore further our technique and test its resilience against the problem of closely spaced particles, we tested its performance with an example of two closely spaced nanoholes. In this case, we use 800 diffraction patterns of two $\lambda/6.33$ nanoholes with center-to-center separation

decreasing from 0.677λ (Rayleigh distance) to 0.158λ (touching) as a test. The Pearson correlation coefficient calculated in Fig. 3b shows that the two nanoholes could be resolved with an accuracy higher than 0.8 across almost the entire range of sub-Rayleigh distances, with a slight drop to 0.75 in the only case of touching nanoholes.

In conclusion, we report on a far-field, single-shot super-resolution optical technique based on the deep learning of the light diffracted on the clusters of subwavelength particles. It allows retrieving maps showing the number, positions, and sizes of the nanoparticles in the cluster and, therefore, constitutes a form of imaging. Our technique is scalable to different wavelengths and film materials as long as the film material is opaque for the wavelength. The image reconstruction accuracy measured as the correlation coefficient between the ground truth and reconstructed maps of the nanoparticles depends on the number of nanoparticles in the largest cluster of sub-Rayleigh spaced particles and varies from 0.82 to 0.71 when the cluster size increases from 2 to 10. In addition, we showed that the technique resolves nanoholes separated significantly smaller than the Rayleigh distance.

Supplementary Material

Supplementary material contains details on: the network (architecture, optimization objectives, hyperparameters and tailored objective functions), the dataset distribution used for training, numerical simulations, performance with noise.

Acknowledgments

This work was supported by the Singapore National Research Foundation (Grant No. NRF-CRP23-2019-0006), the Singapore Ministry of Education (Grant No. MOE2016-T3-1-006), and the Engineering and Physical Sciences Research Council UK (Grants No. EP/T02643X/1).

Data availability

This is the author's peer reviewed, accepted manuscript. However, the online version of record will be different from this version once it has been copyedited and typeset.

PLEASE CITE THIS ARTICLE AS DOI: 10.1063/5.0194393

The data that support the findings of this study are available from the corresponding author upon reasonable request.

References

- ¹ Can Dincer, Richard Bruch, Estefanía Costa - Rama, Maria Teresa Fernández - Abedul, Arben Merkoçi, Andreas Manz, Gerald Anton Urban, and Firat Güder, *Advanced Materials* **31** (30), 1806739 (2019).
- ² Sanyogita Purandare, Jinlong Zhu, Renjie Zhou, Gabriel Popescu, Alexander Schwing, and Lynford L Goddard, *Optics Express* **27** (13), 17743 (2019).
- ³ Silvia Pujals, Natalia Feiner-Gracia, Pietro Delcanale, Ilja Voets, and Lorenzo Albertazzi, *Nature Reviews Chemistry* **3** (2), 68 (2019).
- ⁴ Lothar Schermelleh, Alexia Ferrand, Thomas Huser, Christian Eggeling, Markus Sauer, Oliver Biehlmaier, and Gregor PC Drummen, *Nature cell biology* **21** (1), 72 (2019).
- ⁵ Stefan W Hell and Jan Wichmann, *Optics letters* **19** (11), 780 (1994).
- ⁶ Michael J Rust, Mark Bates, and Xiaowei Zhuang, *Nature methods* **3** (10), 793 (2006).
- ⁷ Eric Betzig, George H Patterson, Rachid Sougrat, O Wolf Lindwasser, Scott Olenych, Juan S Bonifacino, Michael W Davidson, Jennifer Lippincott-Schwartz, and Harald F Hess, *science* **313** (5793), 1642 (2006).
- ⁸ Rucui-Han Jiang, Chi Chen, Ding-Zheng Lin, He-Chun Chou, Jen-You Chu, and Ta-Jen Yen, *Nano Letters* **18** (2), 881 (2018).
- ⁹ Din Ping Tsai and Wei Chih Lin, *Applied Physics Letters* **77** (10), 1413 (2000).
- ¹⁰ Vasily N. Astratov, Yair Ben Sahel, Yonina C. Eldar, Luzhe Huang, Aydogan Ozcan, Nikolay Zheludev, Junxiang Zhao, Zachary Burns, Zhaowei Liu, Evgenii Narimanov, Neha Goswami, Gabriel Popescu, Emanuel Pfitzner, Philipp Kukura, Yi - Teng Hsiao, Chia - Lung Hsieh, Brian Abbey, Alberto Diaspro, Aymeric Legratiet, Paolo Bianchini, Natan T. Shaked, Bertrand Simon, Nicolas Verrier, Matthieu Debailleul, Olivier Haeblerl, Sheng Wang, Mengkun Liu, Yeran Bai, Ji - Xin Cheng, Behjat S. Kariman, Katsumasa Fujita, Moshe Sinvani, Zeev Zalevsky, Xiangping Li, Guan - Jie Huang, Shi - Wei Chu, Omer Tzang, Dror Hershkovitz, Ori Cheshnovsky, Mikko J. Huttunen, Stefan G. Stanciu, Vera N. Smolyaninova, Igor I. Smolyaninov, Ulf Leonhardt, Sahar Sahebdivan, Zengbo Wang, Boris Luk'Yanchuk, Limin Wu, Alexey V. Maslov, Boya Jin, Constantin R. Simovski, Stephane Perrin, Paul Montgomery, and Sylvain Lecler, *Laser & Photonics Reviews* (2023).
- ¹¹ Carolina Rendón-Barraza, Eng Aik Chan, Guanghui Yuan, Giorgio Adamo, Tanchao Pu, and Nikolay I. Zheludev, *APL Photonics* **6** (6), 066107 (2021).
- ¹² T. Pu, J. Y. Ou, V. Savinov, G. Yuan, N. Papisimakis, and N. I. Zheludev, *Adv Sci (Weinh)* **8** (1), 2002886 (2020).
- ¹³ Eng Aik Chan, Carolina Rendón-Barraza, Benquan Wang, Tanchao Pu, Jun-Yu Ou, Hongxin Wei, Giorgio Adamo, Bo An, and Nikolay I. Zheludev, *Nanophotonics* (2023).
- ¹⁴ Olaf Ronneberger, Philipp Fischer, and Thomas Brox, presented at the Medical Image Computing and Computer-Assisted Intervention–MICCAI 2015: 18th International Conference, Munich, Germany, October 5-9, 2015, *Proceedings, Part III* **18**, 2015.
- ¹⁵ Sheng He, Rina Bao, P Ellen Grant, and Yangming Ou, *arXiv preprint arXiv:2304.01401* (2023).
- ¹⁶ Xi Chen, Mikhail E. Kandel, Shenghua He, Chenfei Hu, Young Jae Lee, Kathryn Sullivan, Gregory Tracy, Hee Jung Chung, Hyun Joon Kong, Mark Anastasio, and Gabriel Popescu, *Nature Photonics* **17** (3), 250 (2023).
- ¹⁷ Weihang Zhang, Zhihong Zhang, Liheng Bian, Haoqian Wang, Jinli Suo, and Qionghai Dai, *Optics Letters* **46** (21), 5477 (2021).
- ¹⁸ Jiuxiang Gu, Zhenhua Wang, Jason Kuen, Lianyang Ma, Amir Shahroudy, Bing Shuai, Ting Liu, Xingxing Wang, Gang Wang, and Jianfei Cai, *Pattern recognition* **77**, 354 (2018).
- ¹⁹ Sepp Hochreiter, *International Journal of Uncertainty, Fuzziness and Knowledge-Based Systems* **6** (02), 107 (1998).
- ²⁰ Kaiming He, Xiangyu Zhang, Shaoqing Ren, and Jian Sun, presented at the Proceedings of the IEEE conference on computer vision and pattern recognition, 2016.
- ²¹ John A. Rice, *Mathematical statistics and data analysis*, 3rd ed. (Thomson/Brooks/Cole, Belmont, CA, 2007).